Research Square

Preprints are preliminary reports that have not undergone peer review.
They should not be considered conclusive, used to inform clinical practice,
or referenced by the media as validated information.

Copper-induced suppression of the PPARα–FABP1 axis sensitizes hepatocytes to ferroptosis in Wilson disease

Yingjie Li
The Second Xiangya Hospital of Central South University
Yaoyi Wu
First Hospital of Zhejiang Province: Zhejiang University School of Medicine First Affiliated Hospital
Yanwen Zhou
The Second Xiangya Hospital of Central South University
Liyan Zhao
First Hospital of Zhejiang Province: Zhejiang University School of Medicine First Affiliated Hospital
Zhenyu Xu
The Second Xiangya Hospital of Central South University
Yimin Zhang
First Hospital of Zhejiang Province: Zhejiang University School of Medicine First Affiliated Hospital
Ning Zhou
zhouning1@csu.edu.cn

The Second Xiangya Hospital of Central South University https://orcid.org/0000-0003-2634-8761

Research Article

Keywords: Wilson disease, PPARα–FABP1 axis, Copper overload, Ferroptosis, Lipid peroxidation

Posted Date: February 25th, 2026

DOI: https://doi.org/10.21203/rs.3.rs-8847209/v1

License: This work is licensed under a Creative Commons Attribution 4.0 International License.
Read Full License

Abstract

Wilson disease (WD) is characterized by hepatic copper accumulation and progressive liver injury, yet the mechanisms linking copper overload to hepatocellular damage remain incompletely understood. Here, we identify suppression of the PPARα–FABP1 axis as a key metabolic vulnerability that sensitizes hepatocytes to ferroptosis in WD. Liver tissues from WD patients and *Atp7b*$^{-/-}$ mice exhibited impaired antioxidant capacity, enhanced lipid peroxidation, and coordinated downregulation of PPARα–FABP1 signaling at both transcriptomic and proteomic levels. In hepatocytes, copper exposure induced a time-dependent repression of PPARα and FABP1, lowered the threshold for RSL3-induced ferroptotic cell death, and enhanced lipid peroxidation, effects that were phenocopied by silencing either PPARα or FABP1 and partially rescued by ferroptosis inhibition. Integration of published lipidomic datasets revealed accumulation of peroxidized polyunsaturated fatty acids in WD, while FABP1 overexpression mitigated arachidonic acid–driven lipid peroxidation and ferroptosis. Clinically, hepatic expression and circulating levels of FABP1 declined with disease severity and were associated with inflammatory activity and fibrosis stage in WD patients, showing moderate predictive value for adverse outcomes. Together, these findings establish copper-induced suppression of the PPARα–FABP1 axis as a mechanistic link between metabolic dysregulation and ferroptosis in WD, highlighting a potential therapeutic vulnerability in copper-associated liver disease.

Introduction

Wilson disease (WD) is an autosomal-recessive disorder caused by loss-of-function mutations in ATP7B, leading to impaired biliary copper excretion and progressive copper accumulation, with the liver being a major target organ. Hepatic WD spans a spectrum from asymptomatic aminotransferase elevation to chronic hepatitis, cirrhosis, and acute liver failure, and early mechanistic insight into how copper overload rewires hepatocellular stress responses remains clinically important[1].

Beyond direct protein damage, excessive copper promotes redox imbalance and lipid peroxidation, processes increasingly recognized as central to WD-associated liver injury. Consistent with this concept, targeted lipid mediator/oxylipin profiling in WD patients has revealed broad disturbances in PUFA-derived lipid mediators, supporting the presence of an oxidant lipid milieu in vivo[2]. In parallel, hepatic oxylipin mapping in mouse WD models (including Atp7b deficiency) demonstrates early remodeling of oxidized PUFA products, linking copper overload to enzymatic and non-enzymatic PUFA oxidation within the liver[3]. These observations place oxidized lipids at the intersection of copper toxicity and hepatic inflammation/fibrogenesis in WD[4].

Ferroptosis is an iron-dependent, lipid peroxidation–driven form of regulated cell death characterized by accumulation of oxidized PUFA-phospholipids when antioxidant defenses (notably the glutathione–GPX4 axis) are overwhelmed[5]. Importantly, hepatic ferroptosis has been implicated as a trigger that amplifies inflammatory signaling in steatohepatitis, highlighting the liver's particular vulnerability to lipid peroxide–mediated injury[6]. Given that WD features both oxidative stress and profound lipid remodeling,

ferroptosis provides a compelling mechanistic framework to connect copper-driven lipid peroxidation with downstream inflammatory and fibrotic outcomes.

The reason for hepatocytes in WD become prone to lipid peroxide accumulation remains unclear. Peroxisome proliferator–activated receptor-α (PPARα) is a master transcriptional regulator of hepatic fatty acid uptake and β-oxidation, and its activity coordinates multiple lipid-handling programs[7]. Liver-type fatty acid–binding protein (FABP1; L-FABP) is a prominent PPARα-linked lipid chaperone in hepatocytes, facilitating intracellular trafficking of long-chain fatty acids and modulating nuclear receptor signaling; FABP1 can directly interact with PPARα, supporting functional coupling between this chaperone and the transcriptional lipid program[8]. Beyond transport, FABP1 has been reported to exert antioxidant effects and protect against free-radical damage, suggesting that FABP1 loss could lower the threshold for lipid peroxidation cascades[9]. Notably, multi-omic analyses in WD models indicate broad suppression of metabolic and nuclear receptor pathways under copper overload, providing a mechanistic context in which a PPARα–FABP1 axis could be compromised[10].

Here, we investigate the hypothesis that copper overload suppresses the PPARα–FABP1 axis, leading to impaired lipid metabolic buffering and enhanced susceptibility to ferroptotic lipid peroxidation in WD. We further evaluate the translational relevance by assessing the association between circulating/clinical FABP1 readouts and histologic inflammation/fibrosis severity, and by testing whether FABP1 improves risk stratification for adverse hepatic outcomes in WD.

Methods

Human specimens

This retrospective study involved patients treated at the Department of Infectious Diseases at the Second Xiangya Hospital of Central South University from January 2019 to January 2025. The inclusion criteria encompassed independent cases diagnosed with the hepatic form of WD in accordance with the Leipzig criteria[13], with confirmation via liver biopsy. Exclusion criteria were applied to individuals with other liver diseases, such as MASLD, alcoholic liver disease, viral hepatitis, autoimmune liver diseases, drug-induced liver injury, and other hereditary liver disorders. The study ultimately enrolled 101 non-decompensated WD patients (including chronic liver injury and compensated cirrhosis) with available liver biopsy specimens and blood samples, along with 30 healthy controls who had normal biochemical and metabolic profiles and underwent routine health examinations at the Health Examination Center of The Second Xiangya Hospital during the same period. This experiment was approved by the Medical Ethics Committee of the Second Xiangya Hospital of Central South University, and all procedures were conducted in compliance with the Helsinki Declaration.

Animal cares

Atp7b knockout C57BL/6 mice were obtained from Biocytogen (Suzhou, China) and subsequently bred and maintained at the Experimental Animal Center of Zhejiang Academy of Traditional Chinese Medicine. The mice were housed under controlled conditions: temperature 23 ± 2°C, humidity 45–65%, a 12-hour light/dark cycle, five mice per cage, and free access to food and water. Liver tissue samples were collected when the mice reached 24 weeks of age. All procedures were approved by the Zhejiang Academy of Traditional Chinese Medicine.

Measurement of serum antioxidant and oxidative stress markers

Serum antioxidant capacity and oxidative stress markers were measured using commercial assay kits according to the manufacturers' protocols. Total antioxidant capacity was determined using the Total Antioxidant Capacity Assay Kit (Abcam, Cat# ab65329), with results expressed as Trolox equivalents. Reduced glutathione (GSH) levels were quantified using the Glutathione Assay Kit (Abcam, Cat# ab65322). Lipid peroxidation was assessed by measuring malondialdehyde (MDA) using the Lipid Peroxidation (MDA) Assay Kit (Abcam, Cat# ab118970). All assays were performed using serum samples under standardized conditions, and absorbance was measured with a microplate reader. Concentrations were calculated based on standard curves generated in parallel.

Western Blot Analysis

Western Blot Analysis
Total protein from tissues was extracted using RIPA buffer (Cat. No. P0013C, Beyotime, Beijing, China). For Western blotting, equal protein amounts were separated on 12% SDS-polyacrylamide gels, transferred to nitrocellulose membranes (Cat. No. FFN02, Beyotime, Beijing, China), and blocked with 5% milk. Membranes were incubated overnight with primary antibodies against FABP1 (1:2000, Cat. No. 13626-1-AP, Proteintech, Chicago, USA), Vinculin (1:1000, Cat. No. 66305-1-Ig, Proteintech, Chicago, USA), PPARA (1:1000, Cat. No.15540-1-AP, Proteintech, Chicago, USA), and HRP-conjugated GAPDH (1:5000, Cat. No. HRP-60004, Proteintech, Chicago, USA), followed by a goat anti-rabbit HRP-conjugated secondary antibody (Cat. No. sc-2005, Santa Cruz Biotechnology, Dallas, USA). Protein bands were visualized using ECL (Cat. No. P1008AS, Beyotime, Beijing, China), and expression levels were quantified using ImageJ, with GAPDH as the loading control.

Acid Phosphatase (APH) Assay for Cell Viability

Cell viability was assessed using the acid phosphatase (APH) assay. Briefly, cells were seeded into 96-well plates at the indicated density and allowed to adhere overnight. After experimental treatments, the culture medium was removed, and the cells were gently washed once with phosphate-buffered saline (PBS). Cells were then incubated with APH assay buffer containing p-nitrophenyl phosphate (pNPP) as substrate (100 µL per well) and incubated at 37°C for 90min. The enzymatic reaction was stopped by

adding 20 μL of 1 M NaOH per well, and absorbance was measured at 405 nm using a microplate reader. Cell viability was expressed as a percentage relative to the untreated control group.

RNA-seq analysis

Total RNA was extracted using the RNeasy Kit (QIAGEN, Cat. 74104) from liver tissues of *Atp7b* knockout mice (n = 3) and wild-type controls (n = 3), both groups maintained on a chow diet for 24 weeks. RNA-seq libraries were generated following mRNA enrichment, reverse transcription using random N6 primers, end repair, PCR amplification, and library cyclization. Sequencing was performed on the DNBseq platform, yielding single-end 50bp reads. After filtering, high-quality reads were aligned to the reference genome using Bowtie2, and gene expression levels were quantified using RSEM. Differential gene expression analysis was conducted with DEseq2.

LC-MS/MS analysis

Proteins were extracted by grinding samples in liquid nitrogen, lysed in buffer (8 M urea, 1% protease inhibitor), sonicated, and centrifuged. PTM experiments included TSA (acetylation) and phosphatase inhibitors (phosphorylation). Protein concentration was measured via the BCA assay. Proteins were reduced (DTT), alkylated (IAA), and digested with trypsin (1:50 overnight, 1:100 for 4 hours). Peptides were desalted (C18 SPE), TMT-labeled, pooled, quenched (hydroxylamine), and redesalted. Peptide fractionation was performed using high-pH HPLC, followed by EASY-nLC separation and Orbitrap analysis with a gradient and MS/MS of 25 precursors. Data were processed via Proteome Discoverer (v.2.4) using the Mus musculus database (1% FDR) with modifications (oxidation, acetylation, carbamidomethylation). KEGG tools (KAAS, KEGG Mapper) were used for pathway mapping and enrichment (Fisher's exact test, $p < 0.05$). Heat maps were generated using the R "gplots" package.

SYTOX Green and BODIPY 581/591 C11 staining

Cell death and lipid peroxidation were assessed using SYTOX™ Green and BODIPY™ 581/591 C11 staining. Briefly, cells were incubated with BODIPY 581/591 C11 (Invitrogen, Cat# D3861) at a final concentration of 2 μM in complete culture medium for 30 min at 37°C in the dark. After washing twice with HBSS, cells were incubated with SYTOX™ Green nucleic acid stain (Invitrogen, Cat# S7020) at a final concentration of 1 μM for 10 min at room temperature. Cells were then washed and maintained in phenol red–free medium for immediate imaging or flow cytometric analysis. Fluorescence signals were collected using standard settings.

siRNA-mediated gene silencing

Small interfering RNAs (siRNAs) targeting human PPARA and FABP1 were obtained from Thermo Fisher Scientific (Ambion). Two independent siRNAs were used for each gene (PPARA: siRNA IDs 5348 and

5439; FABP1: siRNA IDs 121193 and 121194). A non-targeting siRNA was used as a negative control (Ambion, Cat# AM4611). Cells were transfected with siRNAs using Lipofectamine™ RNAiMAX according to the manufacturer's instructions. Briefly, cells were transfected at approximately 50–60% confluence with a final siRNA concentration of 20–50 nM. Cells were harvested 24–48 h after transfection for subsequent analyses, and knockdown efficiency was confirmed by immunoblotting.

Transient Elastography

Liver stiffness and hepatic steatosis were assessed using transient elastography (TE) with the FibroScan device (Echosense, France). The measurements were performed with patients lying in a supine position, with their right arm placed behind the head, and under fasting conditions for a minimum of four hours. For each patient, at least ten valid measurements were obtained, and the median value was used for liver stiffness, while CAP values were also recorded to evaluate hepatic fat content. Only results with an IQR/M ratio below 30% were included in the statistical analysis[14].

Histopathological and Immunohistochemical Analysis

Formalin-fixed, paraffin-embedded liver sections were subjected to hematoxylin and eosin (H&E) staining to assess basic histopathological features, including inflammation and fibrosis. Inflammation and fibrosis were evaluated using the Scheuer G/S scoring system[15]. In this system, a score of G ≤ 2 is classified as mild-to-moderate inflammation, while a score of G ≥ 3 indicates severe inflammation. Similarly, a score of S ≤ 2 represents mild to moderate fibrosis, while a score of S ≥ 3 signifies severe fibrosis. For immunohistochemistry, sections were subjected to antigen retrieval in citrate buffer (pH 6.0) at 95°C for 10 minutes, then blocked with hydrogen peroxide. Primary anti-FABP1 antibody (1:400, Cat. No. 13626-1-AP, Proteintech, Chicago, USA), PPARA (1:200, Cat. No.15540-1-AP, Proteintech, Chicago, USA), 4-Hydroxynonenal (1:200, Cat. No.68538-1-Ig, Proteintech, Chicago, USA), and GPX4 (1:200, Cat. No.67763-1-Ig, Proteintech, Chicago, USA)and was applied overnight at 4°C, and sections were subsequently incubated with a secondary antibody, visualized using DAB, and counterstained with hematoxylin.

Serum biochemistry indicators

Serum samples collected during liver biopsies were stored at -80°C and analyzed for FABP1 levels using an ELISA kit (Cat. No.: E-EL-H6153, Elabscience, Houston, Texas). These results were then correlated with liver enzyme and function tests performed in the Central Laboratory of the Second Xiangya Hospital. Blood samples were also immediately processed and analyzed for alanine aminotransferase (ALT), aspartate aminotransferase (AST), complete blood count, and coagulation function. Concurrent plasma samples were collected from both patients and controls using BD anticoagulant tubes, separated, and frozen at -80°C for future analysis.

Statistical Analysis

All analyses were performed using SPSS Statistics for Windows, Version 16.0 (SPSS Inc., Chicago, IL, USA) and GraphPad Prism, Version 8.0 (GraphPad Software, San Diego, CA, USA). Continuous variables

were expressed as mean ± SD and compared using Student's t-test. A two-tailed P value < 0.05 was considered significant. Multiple linear regression was used to identify associations between predictors and outcomes, with model fit assessed using R^2.

Results

Enhanced oxidative stress and lipid peroxidation in WD livers

To assess the redox status and ferroptosis susceptibility in Wilson disease (WD), we first examined liver histology, copper accumulation, and key oxidative stress–related markers. Compared with healthy controls (HC), WD liver sections displayed prominent copper deposition as evidenced by Rhodanine staining, accompanied by reduced expression of the ferroptosis suppressor GPX4 and increased accumulation of the lipid peroxidation product 4-hydroxynonenal (4-HNE) (Fig. 1A).

Consistent with these histological changes, systemic antioxidant capacity was significantly impaired in WD patients. Serum total antioxidant capacity, measured as Trolox equivalent, was markedly decreased in WD compared with HC (Fig. 1B). In parallel, levels of reduced glutathione (GSH), a central intracellular antioxidant and essential cofactor for GPX4 activity, were significantly diminished in WD patients (Fig. 1C). In contrast, malondialdehyde (MDA), a well-established indicator of lipid peroxidation, was substantially elevated in WD (Fig. 1D).

Together, these findings indicate that WD is characterized by compromised antioxidant defenses and excessive lipid peroxidation, creating a cellular environment that is permissive to ferroptotic injury.

Integrated transcriptomic and proteomic analyses identify suppression of the PPARα–FABP1 axis in WD

To elucidate the molecular consequences of hepatic copper overload in Wilson disease (WD), we analyzed liver tissues from *Atp7b*$^{-/-}$ mice. As expected, hepatic copper content was profoundly increased in *Atp7b*$^{-/-}$ mice compared with WT controls, accompanied by a significant elevation in serum ALT levels, indicative of liver injury (Fig. 2A,B).

Transcriptomic profiling revealed extensive metabolic reprogramming in WD livers. KEGG pathway enrichment analysis of downregulated genes demonstrated significant enrichment in lipid- and metabolism-related pathways, including PPAR signaling, fatty acid metabolism, bile secretion, and biosynthesis of unsaturated fatty acids (Fig. 2C). Consistent with these findings, heatmap analysis showed coordinated downregulation of core components of the PPARα–FABP1 axis and genes involved in hepatic lipid handling, including Ppara, Fabp1, Rxra, and lipid droplet–associated and fatty acid oxidation–related genes (Fig. 2D).

Importantly, proteomic profiling independently corroborated these transcriptomic alterations. KEGG enrichment analysis based on downregulated proteins revealed a striking overrepresentation of lipid metabolic pathways in WD livers (Fig. 2E), indicating that copper-induced transcriptional repression is translated into broad suppression at the protein level.

Focusing on key nodal regulators, volcano plot analysis identified FABP1 as one of the most significantly downregulated molecules in WD at both the transcriptomic (Fig. 2F) and proteomic levels (Fig. 2G). These multi-omics findings were further validated by immunoblotting, which confirmed markedly reduced hepatic expression of PPARα and FABP1 in *Atp7b*$^{-/-}$ mice (Fig. 2H).

Collectively, these data demonstrate that hepatic copper overload in WD leads to coordinated suppression of the PPARα–FABP1 axis across transcriptional and proteomic layers, implicating this pathway as a central metabolic node disrupted in WD.

Copper suppresses the PPARα–FABP1 axis and promotes ferroptosis susceptibility in hepatocytes

To determine whether copper directly modulates the PPARα–FABP1 axis and ferroptosis susceptibility, we treated Huh7 hepatocytes with copper. Copper exposure led to a marked increase in intracellular copper accumulation (Fig. 3A) and a modest reduction in basal cell viability (Fig. 3B), indicating cellular stress without overt cytotoxicity.

Notably, immunoblot analysis revealed a time-dependent decrease in both FABP1 and PPARα protein levels following copper treatment (Fig. 3C), suggesting that copper directly suppresses this metabolic axis in hepatocytes.

Functionally, copper-treated Huh7 cells exhibited enhanced sensitivity to the ferroptosis inducer RSL3, as evidenced by a leftward shift in the dose–response curve (Fig. 3D). This effect was partially reversed by co-treatment with the ferroptosis inhibitor Liproxstatin-1, confirming the involvement of ferroptotic cell death.

To further dissect the role of the PPARα–FABP1 axis, we selectively silenced PPARα or FABP1 in Huh7 cells. Knockdown of either gene significantly increased RSL3-induced cell death (Fig. 3E,F). Importantly, silencing of PPARα or FABP1 led to concurrent downregulation of the remaining components of the axis, indicating a tightly coupled regulatory network rather than a linear, unidirectional pathway.

Consistent with these findings, Sytox Green staining demonstrated markedly increased cell death following RSL3 treatment in PPARα- or FABP1-deficient cells, which was substantially attenuated by Liproxstatin-1 (Fig. 3G). Together, these data indicate that copper-mediated suppression of the PPARα–FABP1 axis renders hepatocytes highly susceptible to ferroptosis.

Peroxidized PUFA accumulation couples FABP1 suppression to ferroptosis vulnerability

Given the central role of lipid peroxidation in ferroptosis, we next examined whether accumulation of oxidized polyunsaturated fatty acids (PUFAs) represents a mechanistic link between FABP1 suppression and ferroptosis susceptibility in Wilson disease (WD). Reanalysis of published lipidomic datasets revealed a consistent increase in multiple HETE and HDoHE species in WD patient livers compared with healthy controls (Fig. 4A). Similarly, independent studies in *Atp7b*$^{-/-}$ mice demonstrated marked elevations in hepatic HETE species, supporting the notion that copper overload is associated with enhanced PUFA oxidation in vivo (Fig. 4B).

To directly assess the functional relevance of FABP1 in this context, we overexpressed FABP1 in Huh7 cells, as confirmed by immunoblotting (Fig. 4C). Supplementation with arachidonic acid (AA), a key PUFA substrate for lipid peroxidation, markedly potentiated RSL3-induced cell death, indicating enhanced ferroptosis sensitivity (Fig. 4D). Notably, FABP1 overexpression significantly mitigated AA-enhanced RSL3 cytotoxicity.

Consistent with these viability data, C11-BODIPY staining revealed pronounced lipid peroxidation in cells treated with AA and RSL3, whereas enforced expression of FABP1 substantially reduced lipid ROS accumulation (Fig. 4E). These findings indicate that FABP1 restrains ferroptosis, at least in part, by buffering peroxidizable PUFA substrates and limiting lipid peroxidation.

Clinical downregulation of the PPARα–FABP1 axis correlates with liver injury severity in WD

To assess the clinical relevance of the PPARα–FABP1 axis in Wilson disease (WD), we first examined liver biopsy specimens from patients with different disease severities. Immunohistochemical analysis revealed robust hepatic expression of PPARα, RXRα, and FABP1 in healthy controls, whereas WD livers exhibited a progressive reduction in staining intensity with increasing disease severity, particularly in patients with severe liver involvement (Fig. 5A).

At the systemic level, serum FABP1 concentrations showed a significant positive correlation with platelet count (PLT), a surrogate marker of preserved hepatic function (Fig. 5B), and a significant negative correlation with liver stiffness measurement (LSM), reflecting fibrosis burden (Fig. 5C). Consistently, serum FABP1 levels were markedly reduced in WD patients compared with healthy controls (Fig. 5D). Stratified analyses further demonstrated that FABP1 levels progressively declined with increasing grades of hepatic inflammation (G3–4 vs. G0–2; Fig. 5E) and fibrosis stage (S3–4 vs. S0–2; Fig. 5F).

To explore the potential clinical utility of FABP1 as a biomarker, receiver operating characteristic (ROC) analyses were performed. Serum FABP1 demonstrated moderate discriminatory ability for predicting advanced hepatic inflammation (G) and fibrosis (S), as reflected by the corresponding area under the curve (AUC) values (Fig. 5G,H).

Finally, univariate regression analyses across a panel of clinical and biochemical parameters identified FABP1 as a significant predictor for both inflammatory activity (G) and fibrosis stage (S) in WD (Fig. 5I).

Collectively, these findings indicate that suppression of the PPARα–FABP1 axis is closely associated with disease severity in WD and that circulating FABP1 reflects both inflammatory and fibrotic liver injury.

Discussion

Excessive intracellular copper can cause hepatic pathophysiological changes, including oxidative stress and apoptosis[11,12], autophagy[13], and cuproptosis[14]. In this study, we identify a coherent mechanistic link between copper overload and heightened ferroptosis susceptibility in WD liver, centered on suppression of the PPARα–FABP1 axis. In patient liver specimens, copper accumulation was associated with an antioxidant-deficient, lipid peroxidation–prone state. Consistently, multi-omics analyses of *Atp7b*$^{-/-}$ mice revealed impaired nuclear receptor activity and marked downregulation of the PPARα–FABP1 axis, resulting in compromised lipid toxicity–buffering capacity in vitro. Collectively, these findings uncover a previously unrecognized mechanism underlying ferroptosis vulnerability in WD.

Mechanistically, our findings suggest that copper lowers the ferroptotic threshold by simultaneously impairing GPX4-dependent antioxidant defense and repressing the PPARα–FABP1 metabolic buffering module. Copper exposure suppresses PPARα and FABP1, enhances sensitivity to GPX4 inhibition, and can be rescued by liproxstatin-1. In this framework, attenuation of GPX4 defense in WD liver would be expected to synergize with loss of PPARα–FABP1–mediated lipid handling, thereby promoting lipid peroxide accumulation and tissue injury. A key conceptual advance here is positioning FABP1 not merely as a passive metabolic marker, but as a functional buffer against ferroptotic lipid damage downstream of PPARα. FABP1 is abundant in hepatocytes and has been implicated in intracellular lipid trafficking, detoxification/antioxidant functions, and nuclear receptor ligand handling. In particular, prior mechanistic work demonstrates direct interaction between L-FABP (FABP1) and PPARα and supports a role for FABP1 in facilitating ligand availability and PPARα transcriptional activity[8]. In our system, knockdown of either PPARα or FABP1 reduced the remaining axis components and increased vulnerability to RSL3, indicating positive coupling between these nodes and suggesting that axis collapse can propagate. Conversely, FABP1 overexpression dampened arachidonic acid–driven lipid peroxidation and improved survival under ferroptotic stress. Together, these results support the idea that WD-associated repression of PPARα–FABP1 increases the effective pool of peroxidizable lipids and limits detoxification/handling capacity, thereby amplifying ferroptotic sensitivity when GPX4/GSH defenses are already impaired.

Our data also link WD to a PUFA-oxidation signature consistent with a ferroptosis-permissive lipid environment. Independent lipidomic studies report altered oxylipin patterns in plasma from WD patients and demonstrate broad remodeling of hepatic oxylipins in mouse WD models (including tx-j and *Atp7b*$^{-/-}$), consistent with increased enzymatic and/or ROS-driven oxidation of PUFAs in early stages of hepatic disease. These external datasets complement our in vitro observation that exogenous AA exacerbates RSL3-induced death and increases lipid peroxidation (C11-BODIPY), while FABP1 overexpression counteracts this effect. Because lipoxygenase pathways can contribute to lipid peroxide generation during ferroptosis in certain contexts, the observed oxylipin remodeling may reflect both inflammatory

lipid signaling and enhanced availability of oxidizable substrates[15]. In addition, suppression of PPARα signaling may directly downregulate FABP1 and concomitantly alter GPX4 and ACSL4 expression, thereby promoting ferroptosis. This regulatory axis has also been validated in an IgA nephropathy model, supporting a broader role for PPARα–FABP1–linked lipid handling in ferroptotic susceptibility beyond the liver[16].

Notably, Liu et al.[17] reported that, in gastric cancer, adaptation to a lipid-rich microenvironment suppresses the PPARG–FABP1 axis, limits arachidonic acid uptake, and thereby confers resistance to ferroptosis. We propose that the apparent discrepancy arises from fundamental contextual differences between tumor metabolic adaptation and copper-induced hepatocellular injury. In cancer cells, repression of PPARG–FABP1 appears to be an active, adaptive program that restricts the incorporation of peroxidizable polyunsaturated fatty acids. In contrast, under copper overload, suppression of the PPARα–FABP1 module likely reflects toxic disruption of lipid handling and redox homeostasis, occurring in parallel with impaired GPX4 defense. Thus, rather than limiting substrate availability, FABP1 loss in the copper context may exacerbate lipid dysregulation and oxidative vulnerability, ultimately lowering the threshold for ferroptotic damage.

We also demonstrate that FABP1 is inversely associated with the severity of histologic changes and non-invasive fibrosis assessment in Wilson's disease (WD). Immunostaining for hepatic PPARα/RXRα/FABP1 and serum FABP1 levels are lower in WD patients and decrease progressively with increasing inflammation and fibrosis severity. Serum FABP1 correlates positively with platelet counts and negatively with liver stiffness, and shows moderate predictive performance for inflammation and fibrosis based on ROC analysis. These findings indicate that FABP1 reflects a biologically relevant aspect of the disease rather than simply serving as a generic injury marker, but also acts as a “state marker” of hepatocellular metabolic identity and lipid-buffering capacity in WD, offering potential value for patient stratification and mechanistic endotyping.

Several limitations should be acknowledged. First, while our tissue and biochemical readouts (GPX4 staining, GSH depletion, MDA/4-HNE elevation) and pharmacologic rescue in vitro are strongly consistent with ferroptosis biology, definitive in vivo ferroptosis assignment would benefit from direct quantification of ferroptosis-signature oxidized phospholipids (e.g., oxidized PUFA-PE species) and genetic perturbation of ferroptosis nodes (such as hepatocyte GPX4/FSP1 pathways) in WD models[18]. Second, Huh7 cells are hepatoma-derived and may not fully recapitulate primary hepatocyte copper handling or lipid metabolism; confirming the PPARα–FABP1 dependence of copper-driven ferroptosis sensitization in primary hepatocytes or patient-derived systems will strengthen physiological relevance. Third, the clinical cohort analyses are cross-sectional; longitudinal sampling is needed to determine whether serum FABP1 tracks treatment response, predicts progression, or reflects stage-specific biology (e.g., acute flare vs chronic remodeling). Finally, because WD pathology includes mitochondrial dysfunction, inflammation, and multiple regulated death pathways, future work should clarify how ferroptosis interacts with other copper-triggered stress responses and whether these pathways converge on shared lipid redox vulnerabilities.

In summary, our findings suggest copper overload in WD leads to a dual-hit pro-ferroptotic state. This state is characterized by the depletion of antioxidant defenses, specifically the GSH/GPX4 axis, and the repression of the PPARα–FABP1 lipid-buffering program. Together, these factors increase polyunsaturated fatty acid (PUFA) lipid peroxidation and make hepatocytes more susceptible to ferroptotic injury. Additionally, FABP1 serves as both a functional node that influences vulnerability to lipid peroxidation and a clinically relevant biomarker associated with the severity of inflammation and fibrosis in Wilson's disease.

(A) Representative hematoxylin and eosin (H&E) staining, Rhodanine staining for copper deposition, and immunohistochemical staining of GPX4 and 4-hydroxynonenal (4-HNE) in liver sections from healthy controls (HC) and WD patients. WD livers exhibit marked copper accumulation, reduced GPX4 expression, and increased 4-HNE staining; (B) Serum total antioxidant capacity, expressed as Trolox equivalent (Trolox Eq), was significantly decreased in WD patients compared with HC; (C) Reduced glutathione (GSH) levels were significantly lower in WD patients than in HC; (D) Malondialdehyde (MDA), a marker of lipid peroxidation, was markedly elevated in WD patients.Data are presented as mean ± SEM. ****P < 0.0001 versus HC.

(A) Hepatic copper content was markedly increased in *Atp7b*$^{-/-}$ mice compared with WT controls; (B) Serum alanine aminotransferase (ALT) levels were significantly elevated in *Atp7b*$^{-/-}$ mice, indicating liver injury; (C) KEGG pathway enrichment analysis based on transcriptomic data revealed significant downregulation of lipid- and metabolism-related pathways, including PPAR signaling and fatty acid metabolism, in WD livers; (D) Heatmap showing reduced expression of key genes involved in the PPARα–FABP1 axis and lipid handling in WD compared with normal controls (NC); (E) KEGG pathway enrichment analysis based on proteomic profiling demonstrated that downregulated proteins in WD livers were predominantly enriched in lipid metabolic pathways; (F) Volcano plot highlighting FABP1 as a significantly downregulated gene in the transcriptomic dataset of WD versus NC; (G) Proteomic volcano plot confirming FABP1 as a markedly downregulated protein in WD livers; (H) Immunoblot analysis validating reduced protein expression of PPARα and FABP1 in livers from *Atp7b*$^{-/-}$ mice compared with WT controls. GAPDH served as a loading control. Data are presented as mean ± SEM. ****P < 0.0001 versus controls.

(A) Intracellular copper content was significantly increased in Huh7 cells following copper treatment (50 μM); (B) Copper treatment moderately reduced cell viability in Huh7 cells; (C) Immunoblot analysis showing time-dependent downregulation of FABP1 and PPARα protein levels in Huh7 cells following copper exposure. Vinculin served as a loading control; (D) Dose–response curves demonstrating enhanced sensitivity of Huh7 cells to the ferroptosis inducer RSL3 following copper treatment, which was partially rescued by the ferroptosis inhibitor Liproxstatin-1 (Lipo-1); (E) Cell viability analysis showing increased RSL3-induced cell death in Huh7 cells following knockdown of PPARα or FABP1; (F) Quantification of cell viability confirming that silencing of either PPARα or FABP1 significantly sensitized Huh7 cells to RSL3 (1uM)-induced ferroptotic cell death; (G) Representative Sytox Green staining images

showing increased ferroptotic cell death following PPARα or FABP1 knockdown and RSL3 treatment, which was attenuated by Liproxstatin-1 (2uM). Data are presented as mean ± SEM.

(A) Heatmap summarizing reported increases in hydroxyeicosatetraenoic acids (HETEs) and hydroxydocosahexaenoic acids (HDoHEs) in livers from WD patients compared with healthy controls, adapted from Sergeeva et al; (B) Heatmap showing elevated hepatic HETE species in *Atp7b*$^{-/-}$ mice compared with control groups, adapted from Medici et al; (C) Immunoblot analysis confirming efficient overexpression of FABP1 in Huh7 cells; (D) Cell viability analysis showing that arachidonic acid (AA) supplementation (10uM) markedly enhanced RSL3-induced cell death in Huh7 cells, which was partially rescued by FABP1 overexpression; (E) Representative C11-BODIPY staining images demonstrating increased lipid peroxidation following AA and RSL3 co-treatment, which was attenuated by FABP1 overexpression. Bright-field images are shown below. Data are presented as mean ± SEM. ****P < 0.0001.

(A) Representative immunohistochemical staining of PPARα, RXRα, and FABP1 in liver biopsies from healthy controls (HC) and WD patients with mild or severe liver disease, showing progressive loss of nuclear receptor signaling with disease severity; (B) Correlation analysis showing a positive association between serum FABP1 levels and platelet count (PLT); (C) Correlation analysis showing an inverse association between serum FABP1 levels and liver stiffness measurement (LSM); (D) Serum FABP1 levels were significantly reduced in WD patients compared with HC; (E) Serum FABP1 levels were significantly lower in patients with advanced inflammation (G3–4) compared with those with mild inflammation (G0–2); (F) Serum FABP1 levels were significantly reduced in patients with advanced fibrosis (S3–4) compared with those with mild fibrosis (S0–2); (G) Receiver operating characteristic (ROC) curve evaluating the performance of serum FABP1 in predicting advanced inflammation (G); (H) ROC curve evaluating the performance of serum FABP1 in predicting advanced fibrosis (S3–4 vs. S0–2); (I) Heatmap summarizing univariate regression analyses between FABP1 and clinical parameters for inflammation (G) and fibrosis (S), with color indicating standardized regression coefficients (β). ****P < 0.0001; ***P < 0.001; *P < 0.05.

Declarations

Conflict of interests

All authors have no interest in conflict to be declared.

Ethics approval and consent to participate

This study has been approved by The Medical Ethics Committee of the Second Xiangya Hospital of Central South University and the Animal Welfare Ethics Committee of Zhejiang Provincial Hospital of Traditional Chinese Medicine. All experiments were conducted in accordance with the principles of the Declaration of Helsinki.

Consent for publication

All authors consented to the submission and publication of this study.

Conflict of interests

All authors have no interest in conflict to be declared.

Funding

This work was financially supported by the Key R&D Program of Zhejiang (2022C03125), the National Natural Science Foundation of China (32100597), and the Natural Science Foundation of Hunan Province, China (2022JJ30842)

Author Contributions

Conceptualization, Yingjie Li, Yimin Zhang, and Ning Zhou; Data curation, Yanwen Zhou, Zhenyu Xu, Yaoyi Wu, and Liyan Zhao; Funding acquisition, Yimin Zhang and Ning Zhou; Methodology, Yingjie Li, Yimin Zhang, and Ning Zhou; Project administration, Ning Zhou and Yimin Zhang; Supervision, Ning Zhou and Yimin Zhang; Validation, Yingjie Li, Yanwen Zhou, Zhenyu Xu, Yaoyi Wu, and Liyan Zhao; Visualization, Yingjie Li and Zhenyu Xu; Writing – original draft, Yingjie Li.

Data Availability Statement

The data that support the findings of this study, including animal experiment results and clinical information data without personal identifiers, are available from the corresponding author, Ning Zhou and Yimin Zhang, upon reasonable request.

References

1. Liver European Association for the Study of the, Piotr Socha, Wojciech Jańczyk, et al. EASL-ERN Clinical Practice Guidelines on Wilson's disease. *Journal of Hepatology*. 2025;82(4):690–728. doi:10.1016/j.jhep.2024.11.007
2. Nadezhda V, Azbukina AV, Lopachev DV, Chistyakov et al (2020) Oxylipin Profiles in Plasma of Patients with Wilson's Disease. Metabolites 10(6):222
3. Mazi TA, Shibata NM, Sarode GV et al (2024) Hepatic oxylipin profiles in mouse models of Wilson disease: New insights into early hepatic manifestations. Biochim Biophys Acta Mol Cell Biol Lipids Mar 1869(2):159446. 10.1016/j.bbalip.2023.159446
4. Mazi TA, Shibata NM, Medici V (2020) Lipid and energy metabolism in Wilson disease. Liver Res Mar 4(1):5–14. 10.1016/j.livres.2020.02.002

5. Forcina GC, Dixon SJ (2019) GPX4 at the Crossroads of Lipid Homeostasis and Ferroptosis. Proteomics Sep 19(18):e1800311. 10.1002/pmic.201800311
6. Tsurusaki S, Tsuchiya Y, Koumura T et al (2019) Hepatic ferroptosis plays an important role as the trigger for initiating inflammation in nonalcoholic steatohepatitis. Cell Death Dis Jun 18(6):449. 10.1038/s41419-019-1678-y
7. Burri L, Thoresen GH (2010) Berge. The Role of PPARα Activation in Liver and Muscle. PPAR Res 2010doi. 10.1155/2010/542359
8. Hostetler HA, McIntosh AL, Atshaves BP et al (2009) L-FABP directly interacts with PPARalpha in cultured primary hepatocytes. J Lipid Res Aug 50(8):1663–1675. 10.1194/jlr.M900058-JLR200
9. Yan J, Gong Y, She YM et al (2009) Molecular mechanism of recombinant liver fatty acid binding protein's antioxidant activity. J Lipid Res Dec 50(12):2445–2454. 10.1194/jlr.M900177-JLR200
10. Wooton-Kee CR, Robertson M, Zhou Y et al (2020) Metabolic dysregulation in the Atp7b(-/-) Wilson's disease mouse model. Proc Natl Acad Sci U S A Jan 28(4):2076–2083. 10.1073/pnas.1914267117
11. Liu H, Guo H, Jian Z et al (2020) Copper Induces Oxidative Stress and Apoptosis in the Mouse Liver. Oxid Med Cell Longev 2020:1359164. 10.1155/2020/1359164
12. Liu H, Lai W, Liu X et al (2021) Exposure to copper oxide nanoparticles triggers oxidative stress and endoplasmic reticulum (ER)-stress induced toxicology and apoptosis in male rat liver and BRL-3A cell. J Hazard Mater Jan 5:401:123349. 10.1016/j.jhazmat.2020.123349
13. Zhong CC, Zhao T, Hogstrand C et al (2022) Copper (Cu) induced changes of lipid metabolism through oxidative stress-mediated autophagy and Nrf2/PPARγ pathways. J Nutr Biochem Feb 100:108883. 10.1016/j.jnutbio.2021.108883
14. Tsvetkov P, Coy S, Petrova B et al (2022) Copper induces cell death by targeting lipoylated TCA cycle proteins. Science Mar 18(6586):1254–1261. 10.1126/science.abf0529
15. Shintoku R, Takigawa Y, Yamada K et al (2017) Lipoxygenase-mediated generation of lipid peroxides enhances ferroptosis induced by erastin and RSL3. Cancer Sci Nov 108(11):2187–2194. 10.1111/cas.13380
16. Wu J, Shao X, Shen J et al (2022) Downregulation of PPARα mediates FABP1 expression, contributing to IgA nephropathy by stimulating ferroptosis in human mesangial cells. Int J Biol Sci 18(14):5438–5458. 10.7150/ijbs.74675
17. Liu Y, Tang L, Peng B et al (2025) Gastric cancer adapts high lipid microenvironment via suppressing PPARG-FABP1 axis after arriving in the lymph node. Redox Biol Sep 85:103759. 10.1016/j.redox.2025.103759
18. Kagan VE, Mao G, Qu F et al (2017) Oxidized arachidonic and adrenic PEs navigate cells to ferroptosis. Nat Chem Biol Jan 13(1):81–90. 10.1038/nchembio.2238

Figures

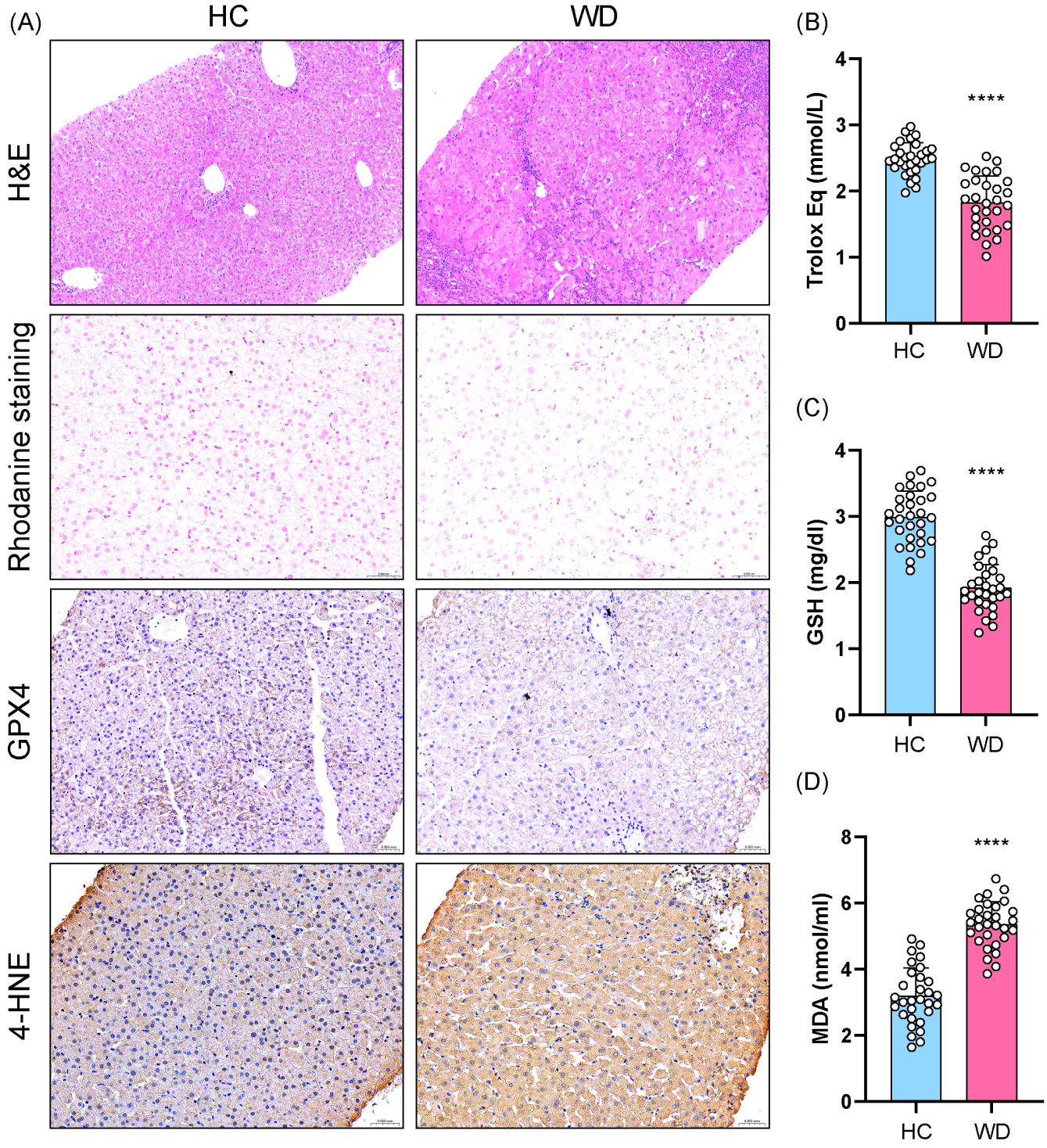

Figure 1

Evidence of impaired antioxidant capacity and enhanced lipid peroxidation in livers from patients with Wilson disease (WD).

(A) Representative hematoxylin and eosin (H&E) staining, Rhodanine staining for copper deposition, and immunohistochemical staining of GPX4 and 4-hydroxynonenal (4-HNE) in liver sections from healthy

controls (HC) and WD patients. WD livers exhibit marked copper accumulation, reduced GPX4 expression, and increased 4-HNE staining; (B) Serum total antioxidant capacity, expressed as Trolox equivalent (Trolox Eq), was significantly decreased in WD patients compared with HC; (C) Reduced glutathione (GSH) levels were significantly lower in WD patients than in HC; (D) Malondialdehyde (MDA), a marker of lipid peroxidation, was markedly elevated in WD patients.Data are presented as mean ± SEM. ****P < 0.0001 versus HC.

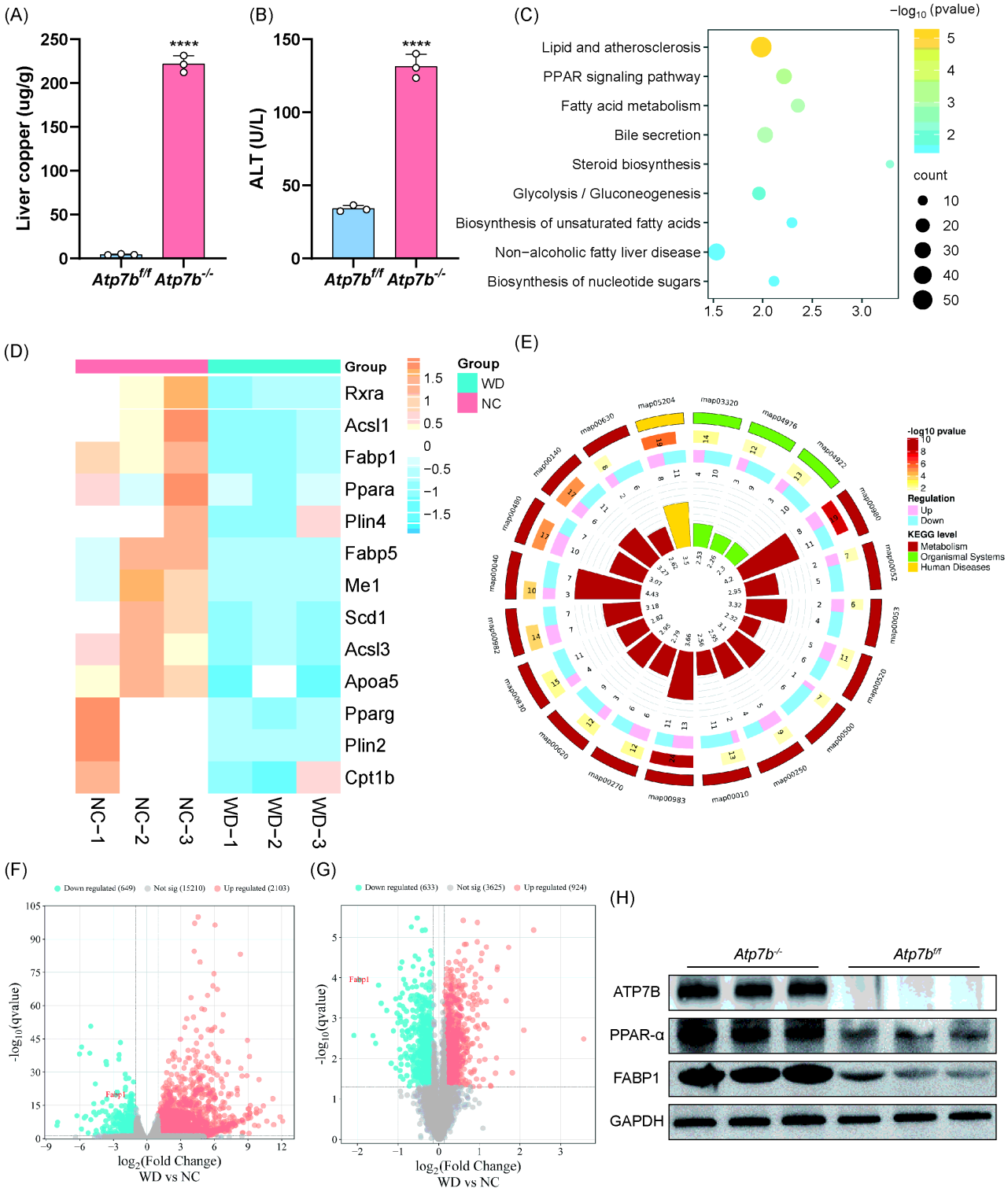

Figure 2

Hepatic copper overload is associated with coordinated repression of the PPARα–FABP1 axis in Wilson disease (WD).

(A) Hepatic copper content was markedly increased in *Atp7b*$^{-/-}$ mice compared with WT controls; (B) Serum alanine aminotransferase (ALT) levels were significantly elevated in *Atp7b*$^{-/-}$ mice, indicating liver injury; (C) KEGG pathway enrichment analysis based on transcriptomic data revealed significant downregulation of lipid- and metabolism-related pathways, including PPAR signaling and fatty acid metabolism, in WD livers; (D) Heatmap showing reduced expression of key genes involved in the PPARα–FABP1 axis and lipid handling in WD compared with normal controls (NC); (E) KEGG pathway enrichment analysis based on proteomic profiling demonstrated that downregulated proteins in WD livers were predominantly enriched in lipid metabolic pathways; (F) Volcano plot highlighting FABP1 as a significantly downregulated gene in the transcriptomic dataset of WD versus NC; (G) Proteomic volcano plot confirming FABP1 as a markedly downregulated protein in WD livers; (H) Immunoblot analysis validating reduced protein expression of PPARα and FABP1 in livers from *Atp7b*$^{-/-}$ mice compared with WT controls. GAPDH served as a loading control. Data are presented as mean ± SEM. ****P < 0.0001 versus controls.

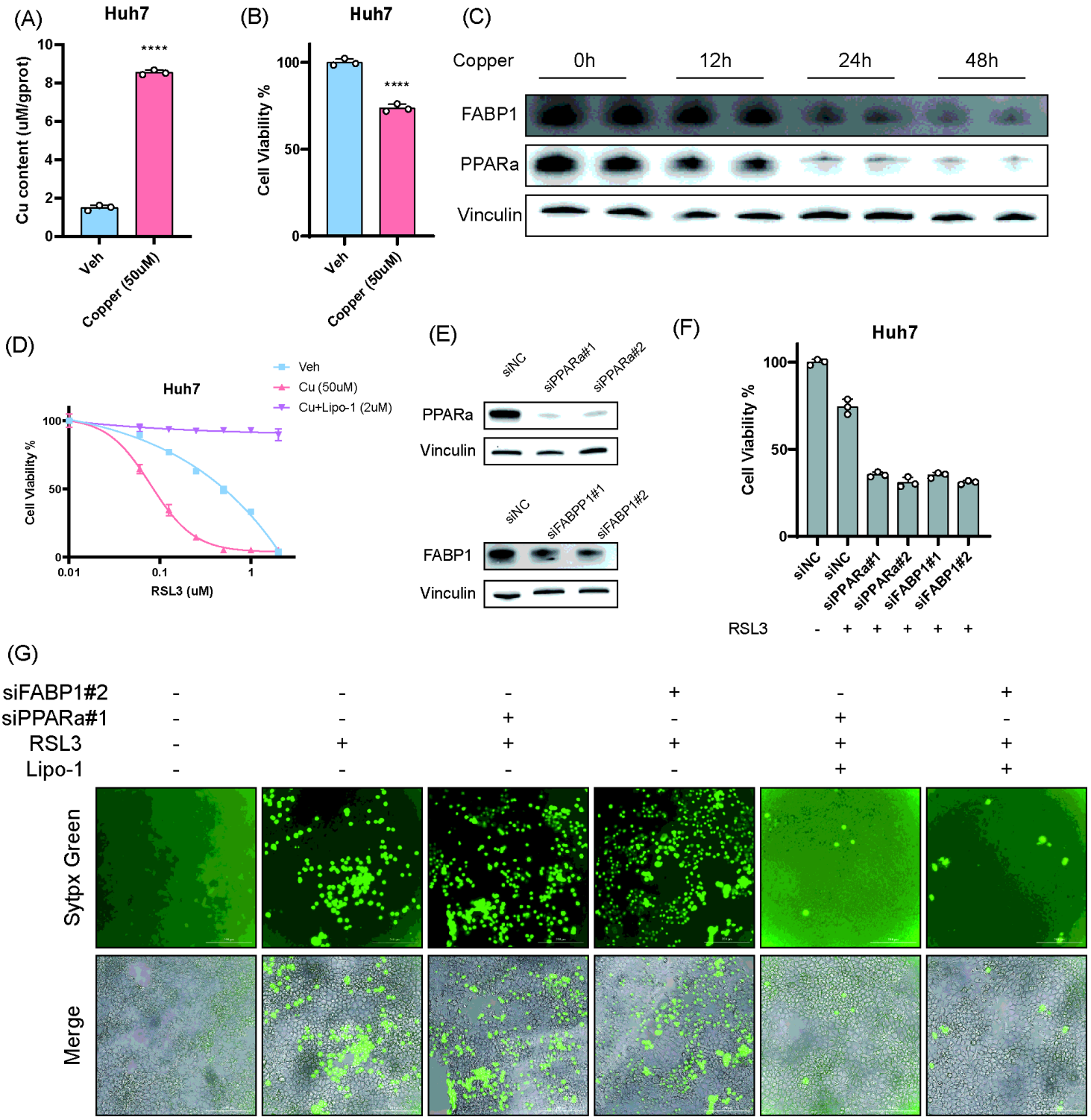

Figure 3

Copper exposure suppresses the PPARα–FABP1 axis and increases ferroptosis susceptibility in hepatocytes.

(A) Intracellular copper content was significantly increased in Huh7 cells following copper treatment (50 μM); (B) Copper treatment moderately reduced cell viability in Huh7 cells; (C) Immunoblot analysis

showing time-dependent downregulation of FABP1 and PPARα protein levels in Huh7 cells following copper exposure. Vinculin served as a loading control; (D) Dose–response curves demonstrating enhanced sensitivity of Huh7 cells to the ferroptosis inducer RSL3 following copper treatment, which was partially rescued by the ferroptosis inhibitor Liproxstatin-1 (Lipo-1); (E) Cell viability analysis showing increased RSL3-induced cell death in Huh7 cells following knockdown of PPARα or FABP1; (F) Quantification of cell viability confirming that silencing of either PPARα or FABP1 significantly sensitized Huh7 cells to RSL3 (1uM)-induced ferroptotic cell death; (G) Representative Sytox Green staining images showing increased ferroptotic cell death following PPARα or FABP1 knockdown and RSL3 treatment, which was attenuated by Liproxstatin-1 (2uM). Data are presented as mean ± SEM.

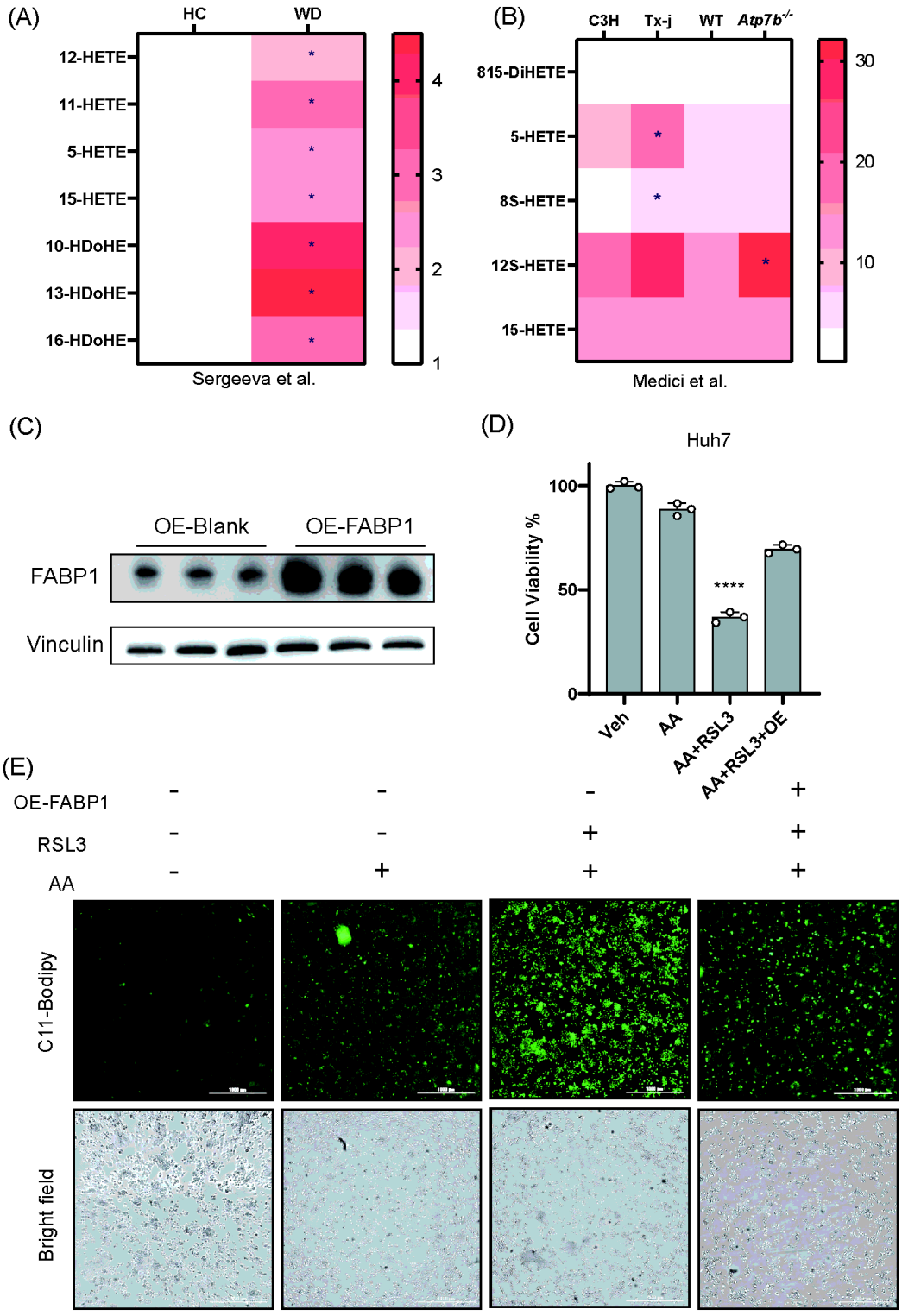

Figure 4

(A) Heatmap summarizing reported increases in hydroxyeicosatetraenoic acids (HETEs) and hydroxydocosahexaenoic acids (HDoHEs) in livers from WD patients compared with healthy controls, adapted from Sergeeva et al; (B) Heatmap showing elevated hepatic HETE species in *Atp7b*$^{-/-}$ mice compared with control groups, adapted from Medici et al; (C) Immunoblot analysis confirming efficient overexpression of FABP1 in Huh7 cells; (D) Cell viability analysis showing that arachidonic acid (AA)

supplementation (10uM) markedly enhanced RSL3-induced cell death in Huh7 cells, which was partially rescued by FABP1 overexpression; (E) Representative C11-BODIPY staining images demonstrating increased lipid peroxidation following AA and RSL3 co-treatment, which was attenuated by FABP1 overexpression. Bright-field images are shown below. Data are presented as mean ± SEM. ****P < 0.0001.

Accumulation of peroxidized polyunsaturated fatty acids (PUFAs) is associated with ferroptosis sensitization in Wilson disease (WD) and is modulated by FABP1.

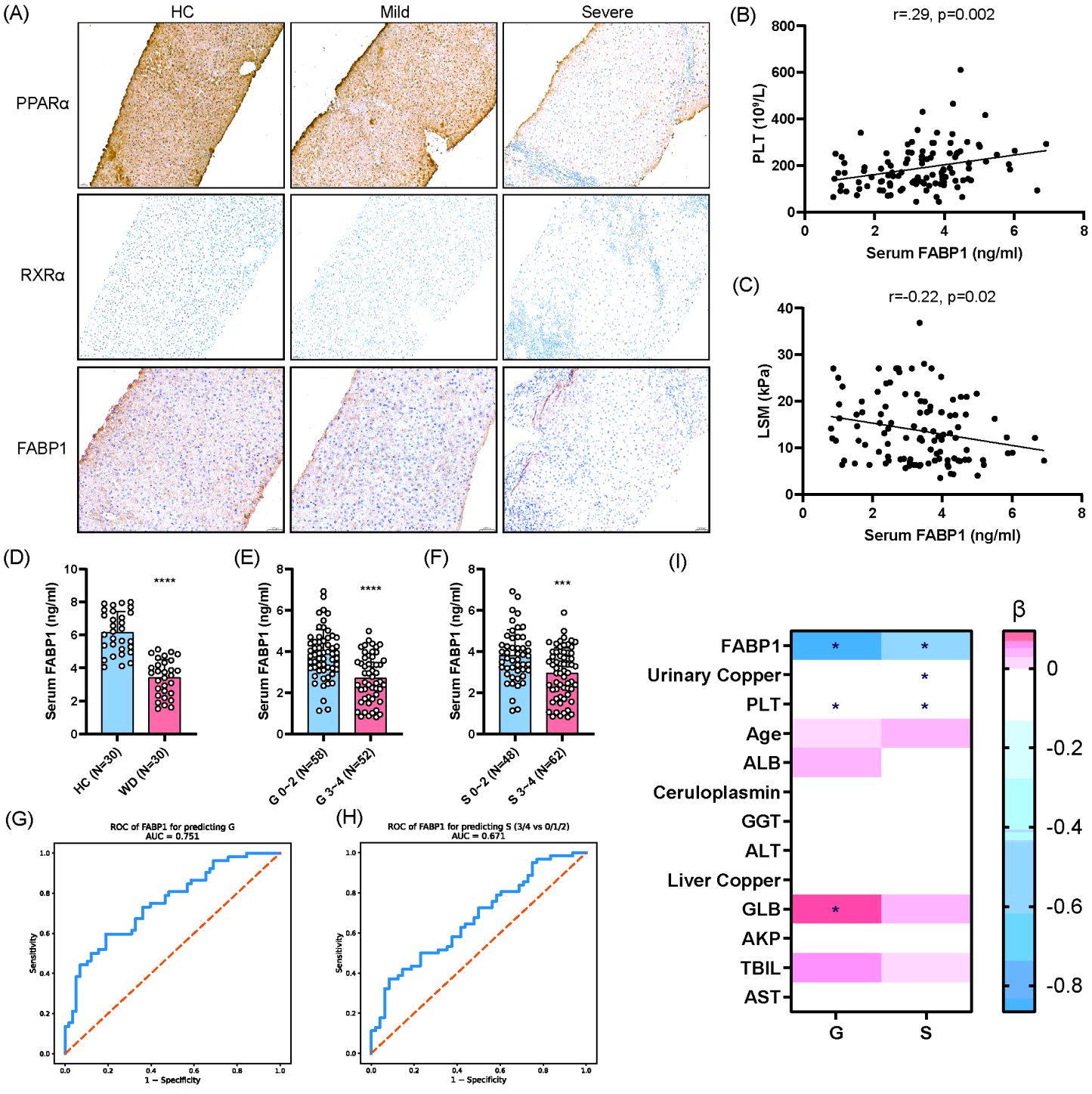

Figure 5

Clinical relevance of FABP1 in Wilson disease (WD).

(A) Representative immunohistochemical staining of PPARα, RXRα, and FABP1 in liver biopsies from healthy controls (HC) and WD patients with mild or severe liver disease, showing progressive loss of nuclear receptor signaling with disease severity; (B) Correlation analysis showing a positive association between serum FABP1 levels and platelet count (PLT); (C) Correlation analysis showing an inverse association between serum FABP1 levels and liver stiffness measurement (LSM); (D) Serum FABP1 levels were significantly reduced in WD patients compared with HC; (E) Serum FABP1 levels were significantly lower in patients with advanced inflammation (G3–4) compared with those with mild inflammation (G0–2); (F) Serum FABP1 levels were significantly reduced in patients with advanced fibrosis (S3–4) compared with those with mild fibrosis (S0–2); (G) Receiver operating characteristic (ROC) curve evaluating the performance of serum FABP1 in predicting advanced inflammation (G); (H) ROC curve evaluating the performance of serum FABP1 in predicting advanced fibrosis (S3–4 vs. S0–2); (I) Heatmap summarizing univariate regression analyses between FABP1 and clinical parameters for inflammation (G) and fibrosis (S), with color indicating standardized regression coefficients (β). ****P < 0.0001; ***P < 0.001; *P < 0.05.

Supplementary Files

This is a list of supplementary files associated with this preprint. Click to download.

- KeyMessages.docx
- UncroppedWesternBlotImages.tif